thickness less than 14 km; continental cover has thickness varying from 24 km up to more than 38 km; and cover of transitional zones has thickness value from 14 to 24 km.

The Vietnam territory and its adjacent areas seismic lithosphere does not pick out for all territory. On the whole, thickness of the lithosphere of Vietnam territory and its adjacent areas is varying from 50 km to larger 110 km. The seismic lithosphere picks up under central part of North Calimantan block up to 50 km, under South China block up to 75 km, under Indochina block up to 50 km. The maximum lithosphere depth is under blocks Central East Sea and East East Sea — 110÷120 km.

References

Geyko V. S. A general theory of the seismic travel-time tomography // Geophys. J. — 2004. — **26**, № 2. — P. 3—32.

Cao Dinh Trieu. Geophysical fields and lithosphere structure of Vietnam territory // Publishing house Science and Technology. — Hanoi, 2005. — P. 330 (in Vietnamese).

Autowave solutions of a nonlocal model for geophysical media taking into account the hysteretic character of their deformation

© ***V. Danylenko, S. Skurativskyy, 2010***

Division of Geodynamics of Explosion, Institute of Geophysics,
National Academy of Sciences of Ukraine, Kiev, Ukraine
skurserg@rambler.ru

Geophysical media as open thermodynamic systems actively display synergetic properties, ability to creation of localized dissipative structures, and an order. Experimental investigations show that dynamics of physical processes in nonequilibrium media is determined substantially by hierarchy and discreteness of a media structure, the set of internal relaxing processes, the nonlocality of interaction between structure elements, the directed exchange of energy between the degrees of freedom. In the papers [Danylenko, Skurativsky, 2007; Danylenko et al., 2008] it is proposed to take into account these features of internal media structure in the dynamical equation of state. This leads to the nonlocal nonlinear mathematical model for structured media:

$$\frac{d\rho}{dt}+\rho\frac{\partial u}{\partial u}=0\,,\quad \rho\frac{du}{dt}+\frac{\partial p}{\partial u}=\gamma\rho^m\,,$$

$$\tau\left(\dot p-\chi\dot\rho\right)=æ\rho^n-p+\Phi_1+\sigma\left\{p_{xx}+\rho^{-1}p_x\rho_x-\eta\left(\rho_{xx}-\rho^{-1}\rho_x^2\right)\right\}-$$

$$-h\left(\ddot p+\eta\left\{2\rho^{-1}\dot\rho^2-\ddot\rho\right\}\right)+\frac{h^2}{\tau}\dddot p+\frac{h\chi}{\tau}\left\{\frac{6}{\rho}\dot\rho\ddot\rho-\frac{6}{\rho^2}\dot\rho^3-\dddot\rho\right\}\,, \qquad (1)$$

where ρ is the density of a medium, u is the velocity, p is the pressure, $\gamma\rho^m$ is the external mass force, τ is the relaxing time, σ and h are parameters of spatial and temporal nonlocalities, the parameters æ and χ are proportional to the squares of equilibrium and frozen speeds of the sound. The function $\Phi_1=\varepsilon\Phi_1\left(\rho,p,\dot\rho,\dot p\right)$ describes hysteretic reaction of a medium under the deformation, ε is the scale parameter.

Previous investigations of the wave solutions of model (1) in the form [Danylenko, Skurativsky, 2009]

$$\rho=R(\omega)\,,\quad p=P(\omega)\,,\quad u=2\xi t+U(\omega)\,,\quad \omega=x-\xi t^2 \qquad (2)$$

shown that accounting the spatial and temporal nonlocal effects in the dynamical equation of state ex-

pands substantially the class of solutions in comparison with the local model (τ, σ, h are infinitesimal). In particular, the set (2) contains periodic, quasiperiodic, multiperiodic, and chaotic regimes, which are connected with each other by means of bifurcational scenarios. The solitary waves with the oscillating asymptotics were discovered as well.

Thus, basing upon the results of investigations of models that do not take into account the hysteretic character of media deformations, we shall study the influence of the hysteretic function Φ_1 in the dynamical equation of state on the structure of solutions (2). The function Φ_1 describes the histeretic loop in the plane (ρ; p) under the harmonic loading. The form of this loop is defined by the following relation

$$\Phi_1 = \begin{cases} \exp\left(C_2\{\rho-\rho_0\}\right)-1, \ \rho \ge \rho_0, \ d\rho/dt \ge 0, \\ \left[\exp\left(C_2\{\rho_{\max}-\rho_0\}\right)-1\right]\dfrac{\exp\left(C_1\{\rho-\rho_0\}\right)-1}{\exp\left(C_1\{\rho_{\max}-\rho_0\}\right)-1}, \ \rho \ge \rho_0, \ d\rho/dt < 0, \\ -\left[\exp\left(-C_2\{\rho-\rho_0\}\right)-1\right], \ \rho < \rho_0, \ d\rho/dt \le 0, \\ -\left[\exp\left(C_2\{\rho_{\max}-\rho_0\}\right)-1\right]\dfrac{\exp\left(-C_1\{\rho-\rho_0\}\right)-1}{\exp\left(C_1\{\rho_{\max}-\rho_0\}\right)-1}, \ \rho < \rho_0, \ d\rho/dt > 0, \end{cases} \tag{3}$$

where $C_2<C_1$. In the case, when $C_2<C_1$, the area bounded by the loop is zero. We should note that the set of enclosed loops appears in the plane (ρ; p) instead of one loop, if we use the loading, distinct from harmonic one. The elements of function (3) can be used for description of the simplest cases of enclosed loops (Fig. 1).

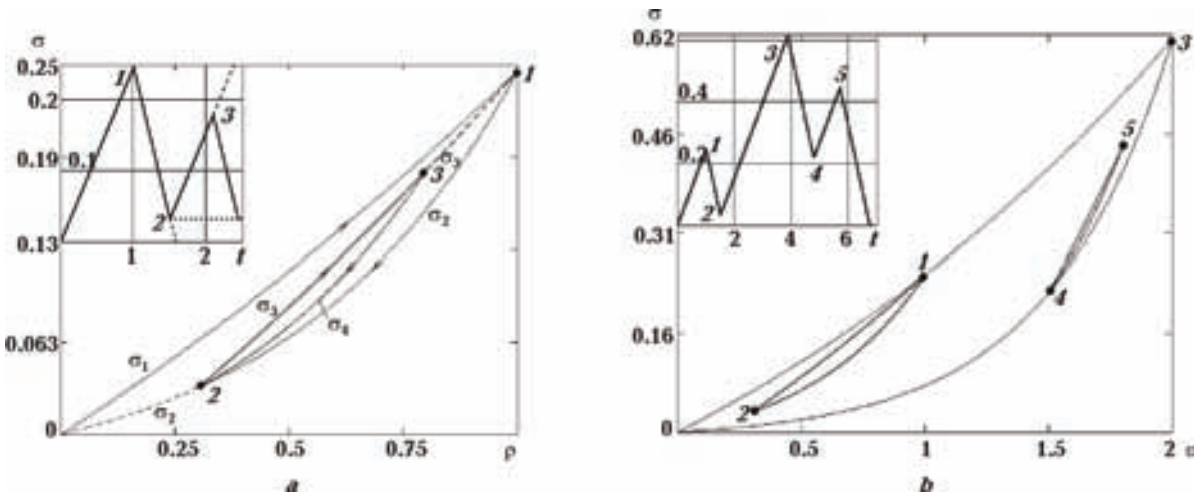

Fig. 1. The construction of two (*a*) and three (*b*) encloset histeretic loops in the plane (ρ; p).

Substituting solution (2) into system (1), we obtain the quadrature $UR=S=\text{const}$ and the dynamical system:

$$R' = W, \ P' = \gamma R^m - 2\xi R = \frac{S^2}{R^2}W, \ W' = Z, \ Z' = \frac{F + R^7\varepsilon\Phi_1}{bS^3\left(\chi - S^2\right)R^2}. \tag{4}$$

Here $\left(\circ\right)' = d\left(\circ\right)/d\omega$, $F = F\left(R,P,W,Z\right)$ is the nonlinear function. The analitical expression for the function F is omitted due to its length. Note that analitical expression (3) for the histeretic loop can also be written in terms of invariant variables (2).

Nonlinear dynamical system (4) is investigated by means of the qualitative and numerical methods. Equating the right parts of system (4) to zero, we get the coordinates of the fixed point

$$R_0 = \left(2\xi/\gamma\right)^{1/m-1}, \quad P_0 = æR_0^n, \quad W_0 = 0, \tag{5}$$

which do not depend on the parameters of the histeretic function Φ_1. Analyzing the stability of fixed point (5) under the neglecting the histeretic function Φ_1 we state that at $\chi = 16$; $S = 3.2$; $\tau = 1$; $æ = 0.9$; $\zeta = -0.5$; $h = 6.74$; $\sigma = 0$; $\gamma = -0.6$; $n = 4$; $m = 8$; $b = -3.8$ the fixed point changes the type from unstable node-focus to stable one. In the vicinity of fixed point (5) the unstable limit cycle appears at increasing the parameter h. Bifurcational analysis of dynamical system (4) in the case when $\Phi_1 \neq 0$ and zero area of histeretic loop shown that for $C_2 = C_1 > 0$ fixed point (5) is a stable node-focus surrounded by both unstable and stable cycles. Consider the case, when $C_1 \neq C_2$ and function (3) describes the loop with nonzero area. Then as a consequence of histeretic loop including the structure of the phase space of system (4) becomes more complicated at increasing the parameter C_1. In particular, at $C_2 = 7.5$; $C_1 = 27$ there are several localized and separated regimes in the phase space of dynamical system (4), namely, fixed point (5), both stable and unstable cycles surrounding it (Fig. 2, *a*), and the chaotic attractor in addition (Fig. 2, *b*). Note that the chaotic attractor does not exist neither at $C_1 = C_2 = 7.5$ nor at $C_1 < C_2 = 27$. So that the chaotic attractor is created due to accounting the histeretic loop.

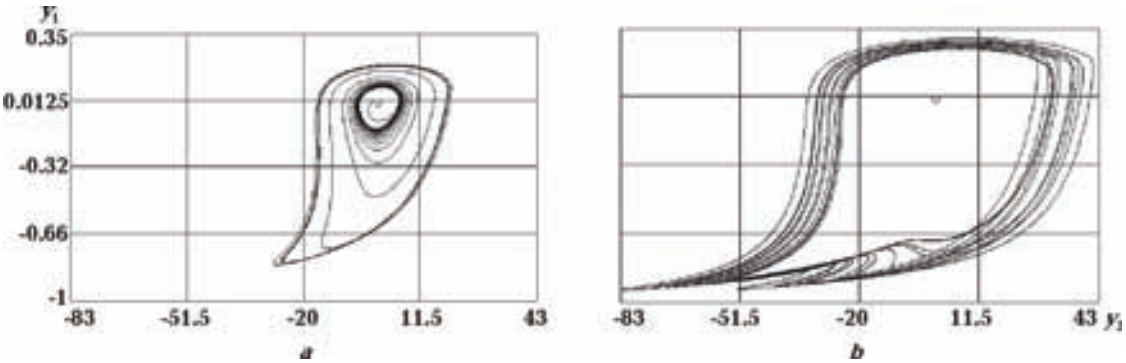

Fig. 2. The structure of the phase space of system (4) at C_1=27 (*a*) and C_2=7.5 (*b*).

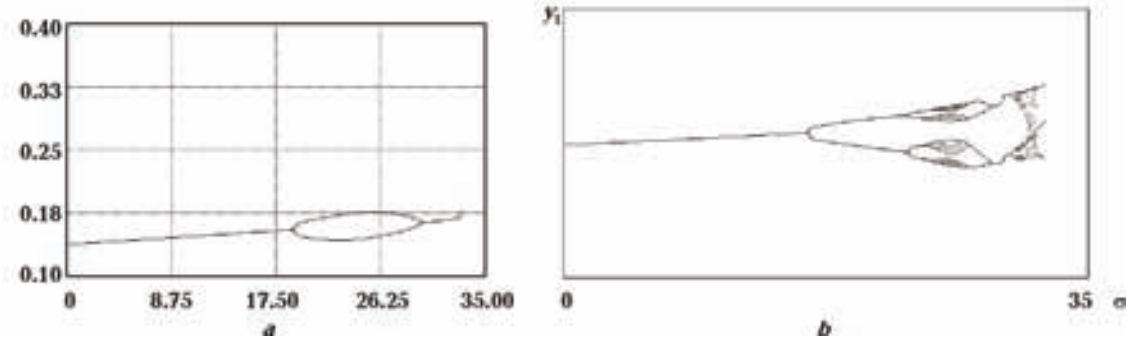

Fig. 3. Poincare diagrames of the limit cycle development at increasing σ: *a* — C_1=C_2=9.5; *b* — C_2=9.5, C_1=19.

Another manifestation of the histeretic function Φ_1 adding is regularization of chaotic oscillations. According to the numerical experiments, at $S = 3.8$, $C_1 = C_2 = 7.5$, $\varepsilon = 0{,}1$ the complicated periodic trajectory exists in the vicinity of the fixed point. Analyzing the development of the periodic trajectory by Poincare diagram we show that the period doubling cascade with chaotic attractor creation is actualized at $C_1 \in [7.5;\ 8]$. But if we fix $C_2 = 7.5$ and vary $C_1 \in [7.5;\ 8]$, then the periodic regime exists only instead of the chaotic attractor.

The existence of new wave regimes for model (1) is connected with the effects of spatial nonlocality, which are described by terms with the parameter σ. Analyzing the Poincare diagram of the limit cycle

development at increasing σ and $C_1 = C_2$ (zero loop area) we see that the size of *T*-period cycle is growing and there is an interval of σ corresponding to the existence of 2*T*-period cycle (Fig. 3, *a*). The structure of solutions (2) is much more complicated in the case of nonzero histeretic loop area at $C_2 = 9{,}5$, $C_1 = 19$. Studying the Poincare diagram in picture 3b we can distinguish several period doubling cascade, intervals of the different type chaotic attractor existence, moment of the histeretic transition from one attractor to other.

Thus, the accounting a histeretic loop in the dynamical equation of state causes new wave regimes creation. The histeretic loop is the way of elastic energy utilization and in the same time it is the nonlinear element of media, which can cause unstability generation in media and produce localized dissipative structures.

References

Danylenko V. A., Danevich T. B., Skurativskyy S. I. Nonlinear mathematical models of media with temporal and spatial nonlocalities. — Kiev: Institute of Geophysics NAS of Ukraine, 2008. — 86 p. (in Russian).

Danylenko V. A., Skurativskyy S. I. Autowave solutions of a nonlocal model of geophysical media with regard for the hysteretic character of their deformation // Rep. of the NAS of Ukraine. — 2009. — **1**. — P. 98—102 (in Ukrainian).

Danylenko V. A., Skurativskyy S. I. Invariant chaotic and quasi-periodic solutions of nonlinear nonlocal models of relaxing media // Rep. on Math. Phys. — 2007. — **59**. — P. 45—51.

What does Grace satellite mission tell us about seismic cycle?

© ***M. Diament[1], V. Mikhailov[2,1], I. Panet[3,1], F. Pollitz[4], 2010***

[1]Institut de Physique du Globe de Paris, Université Paris-Diderot, Paris, France
diament@ipgp.fr
[2]Institute of Physics of the Earth, RAS, Moscow, Russia
mikh@ifz.ru
[3]Institut Geographique National, Laboratoire LAREG, Marne-la-Vallée, France
panet@ign.fr
[4]U.S. Geological Survey, California, USA

Launched in March 2002, the GRACE mission measures the temporal variation of the gravity field at a spatial resolution of about 400 km, and at a temporal resolution from ten days to one month.

These information complements ground based geodetic and geophysical ones. The temporal variations of the Earth gravity field are dominated by the effect of the water circulation between the atmosphere, the oceans, the land hydrological systems and the polar ice caps. Such mass redistributions cause geoid variations of a few millimetres at various temporal and spatial scales. Locally, large seismic events also generate geoid variations of similar amplitude, which may also be detectable by GRACE [Gross, Chao, 2001; Mikhailov et al., 2004; Sun, Okubo, 2004; de Viron et al., 2008].

One of the largest earthquakes in recent decades, the M_w 9.2 Sumatra-Andaman, earthquake, occurred on December 26th 2004 at a particularly complex subduction boundary, along which the Indian and Australian plates subduct below a set of microplates comprising the forearc sliver plate, the Burma and the Sunda ones. The Sumatra-Andaman earthquake ruptured at least 1300 km of this subduction boundary. It was followed by numerous aftershocks and by a second very large earthquake, the M_w 8.7 Nias earthquake, on March 28th, 2005. During the following years, slip at depth has continued, as showed by the sequence of recorded aftershocks and regional GPS data.

The December 2004 Sumatra-Andaman event is associated with a large gravity co-seismic anomaly in the Andaman Sea and very fast post seismic relaxation that is well monitored by Grace [Panet et al., 2007; 2010]. This gravity variation is due to vertical displacement of density interfaces (mostly the